

# Proving the curvature-induced frequency asymmetry of spin-wave modes in magnetic nanotubes with coplanar wave guides

J. A. Otálora,<sup>1, a)</sup> A. Kákay,<sup>2</sup> H. Schultheiss,<sup>2</sup> K. Lenz,<sup>2</sup> A. Thomas,<sup>1</sup> and K. Nielsch<sup>1,3</sup>

<sup>1)</sup> Institute of Metallic Materials at the Leibniz Institute for Solid State and Materials Research, IFW, 01069 Dresden, Germany

<sup>2)</sup> Helmholtz-Zentrum Dresden-Rossendorf, Institute of Ion Beam Physics and Materials Research, Bautzner Landstr. 400, 01328 Dresden, Germany

<sup>3)</sup> Technische Universität Dresden, Institute of Materials Science, 01062 Dresden, Germany

(Dated: 10 February 2022)

We calculate the optimal conditions to quantify curvature-induced nonreciprocity in the dispersion relation of a magnetic nanotube by calculating the coupling impedance between spin waves modes of the nanotube and Coplanar Wave Guides (CPWs). We calculate the system parameters to quantify the curvature-induced frequency asymmetry up to GHz orders, and the changes on the asymmetry up to the same GHz range when a magnetic field  $\mu_0|H_z| < 60$  mT is applied along the large nanotube axis. Moreover, we show the feasibility of the CPWs to excite higher order SW modes with wavelengths down to few hundred of nanometers, which could be used to encode information not only in the longitudinal SW phase but also in the azimuthal one, therefore paving the way towards technologies that increases the density and fidelity of information transfer, as well as for encouraging technological development of 3D magnonic devices.

Magnonics, the field that harnesses spin waves (SWs) and magnons (their quanta) as the information carrier, promises an unprecedented augment of capabilities for information transfer, processing and sensing. Over macroscopic propagation distances without electron charges being displaced, SWs pave the way towards energy-efficient technologies that circumvent the crisis caused by the overheating of modern complementary metal oxide semiconductor (CMOS) technology.<sup>1–5</sup> Indeed, applications employing magnons have been highlighted by their lower power consumption, reconfigurable multi-functionality, faster operation rates, and by its potential integrability to spintronic and electronic environments via the interconversion mechanisms among magnons, spin accumulation and electric charge.<sup>6–10</sup> The magnon transistor for all-magnon data processing,<sup>11</sup> SW multiplexers,<sup>12</sup> magnonic beam splitter,<sup>13</sup> magnonic diodes,<sup>14</sup> SW logic gates<sup>15–17</sup> and phase-to-amplitude/amplitude-to-phase SW converters<sup>18–20</sup> are just a few illustrative examples for magnonic devices.

Up to now, magnonics focuses on two-dimensional (2D) planar geometries. Additional degrees of freedom can be obtained in three dimensional (3D) curved magnetic membranes. Indeed, curved membranes expand the toolbox of SW interactions with curvature-induced magnetochiral effects, which can be exploited for further enhancements of magnonic devices capabilities.<sup>23–32</sup> Among the family of curvilinear 3D architectures like toroids, helixes, möbius rings and spherical shells,<sup>28</sup> we focus here on the tubular geometry due to their predicted curvature-induced non-reciprocities in SW transport.<sup>21,25,27,32</sup>

Despite the predicted curvature-induced magnetochiral effects in SWs, so far there is no experimental evidence of the nonreciprocities in magnetic nanotubes (MNTs). Accordingly, in this paper, we calculate theoretically the optimal parameters of a magnonic device that can be further implemented to confirm and quantify experimentally the curvature-induced non-reciprocities of SWs. We consider a nanotubular structure placed on two coplanar waveguides (CPWs) from which magnons are excited in the nanotube and collected via impedance measurements (see figure 1b). The nanotubular structure consists of a core-shell magnetic nanowire (CSNW)<sup>29</sup> made of an inner conductor non-magnetic wire, covered by an intermedium separator shell and an outer magnetic membrane (see figure 1a). For theoretical modeling, the CSNW is treated as a simple MNT with its equilibrium magnetic configuration in a homogeneous helical state (figure 1c).<sup>21,22</sup> Such an equilibrium state characterized by the angle  $\Theta_0$  can be stabilized by simultaneously applying azimuthal and longitudinal fields,  $H_0$  and  $H_z$ , respectively.<sup>33</sup> The field  $H_0$  is induced by an electric current  $j$  that is injected to the internal conductor wire.<sup>21,33</sup>

We model the feasibility to observe, via impedance response of the CPWs, the curvature-induced GHz-range frequency shift in the dispersion relation and its controllability by the application of  $H_z$ . We calculate the efficiency to observe nonreciprocities of the fundamental and higher modes, the latter characterized by their non-homogeneous azimuthal phase distribution. It is worth noticing that exciting higher SW modes are possible due to the non-homogeneous profile of the rf-field produced by the CPW along the azimuthal direction  $\hat{\varphi}$  in the MNT mantle, as we see later.

In the following, analytical results are presented assuming a permalloy nanotube with outer(inner) radius  $R = 105$  nm ( $r = 95$  nm), length  $L = 15$   $\mu\text{m}$ , saturation

<sup>a)</sup> Corresponding author: j.otalora@ifw-dresden.de

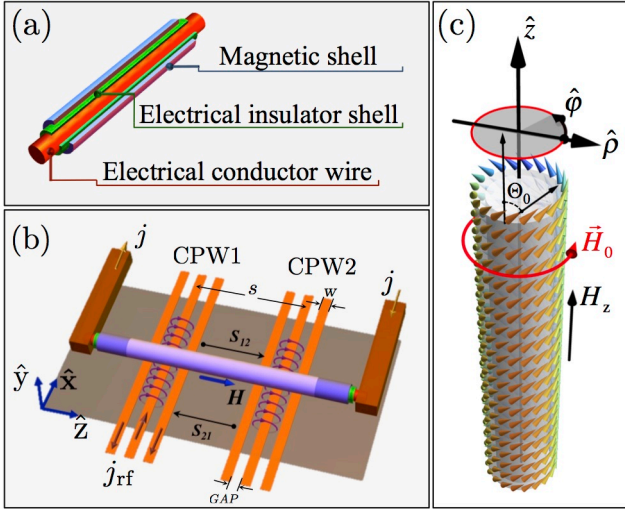


FIG. 1. (Color online). Illustration of the three dimensional curvilinear magnonic transducer. (a) The magnonic component is given by a core-shell magnetic nanotube (CSMNT) made of an internal conductor wire, and electrical insulator layer and an outer magnetic shell. (b) The CSMNT is placed on top of two identical and parallel coplanar wave guides (CPWs) denoted by CPW1 and CPW2. Each of the CPWs consists of two outer ground and a inner signal conductors, separated by a gap  $GAP$  (inner conductor width  $w_{ic}$ , outer conductor width  $w_{oc}$  and  $GAP$  have the same dimension  $GAP = w = w_{ic} = w_{oc}$ ). The waveguides are placed at a distance  $s$  from each other and are shorted at one end of the transmission region. The internal conductor wire is connected to two electrical terminals for the injection of a DC electric current  $j$ , which creates a circular magnetic field  $H_0$  in the magnetic shell. A radio-frequency electrical current  $j_{rf}$  is injected along the CPW in order to generate a radio-frequency magnetic field that excites the SWs in the nanotube. Therefore, one CPW excite SWs that propagate towards the other CPW inducing a signal. This signal will be measured via the transmission coefficients  $S_{12}$  and  $S_{21}$ . c) The nanotube is assumed in a helical configuration describe by the angle  $\Theta_0$ .<sup>21,22</sup>

magnetization  $\mu_0 M_s = 1$  T, exchange stiffness constant  $A = 13$  pJ/m and exchange length  $l_{ex} = 5.8$  nm. The equilibrium state for these material parameters and geometrical dimension in the absence of external fields is given by a homogeneously magnetized body along the long axis with two oppositely curling vortex caps at the ends.<sup>34-37</sup> The critical field to stabilize the circular magnetic state is  $\mu_0 H_{\text{crit}} \approx 1.2$  mT.<sup>21</sup> Therefore, in order to set the magnetization in this circular state a circular field strength of  $\mu_0 H_0 = 5$  mT is assumed. Inducing this field value requires the injection of a minimum amount of electric current  $j$  as is discussed in the supplementary material.<sup>33</sup>

The application of  $\vec{H}_z = H_z \hat{z}$  simultaneously with  $H_0$  stabilizes the helical magnetization state,<sup>21,22</sup> which can be described with the angle  $\Theta_0$  (see figure 1c).

This angle must accomplish the equilibrium condition  $(H_0 - H_u \sin \Theta_0) \cos \Theta_0 - H_z \sin \Theta_0 = 0$ ,<sup>33</sup> where  $H_u = M_s l_{ex}^2 / b^2 \geq 0$  is the exchange field arising from twisting the equilibrium magnetization along the azimuthal direction  $\hat{\varphi}$ ,  $b^{-2} = 2\pi \log(R/r)/S$ ,  $S = \pi(R^2 - r^2)$  is the cross-section area of the magnetic shell and  $M_s$  is the saturation magnetization. Under the condition  $H_0 > H_u$ , the helical state is stabilized, therefore the angle  $\Theta_0$  evolves monotonically among  $\Theta_0 = -\pi$  at very large negative values of  $H_z$  (pointing to the  $-\hat{z}$  direction), passing through  $\Theta = \pi/2$  at  $H_z = 0$  and going to  $\Theta_0 = 0$  at very large positive values of  $H_z$  (pointing to the  $\hat{z}$  direction). During this evolution no hysteresis is presented, i.e. negligible coercive/switching fields.

The dispersion relation  $f[n, k_z] = \omega_{k_z}^n / (2\pi)$  and dynamic susceptibility  $\aleph_{k_z}^n$  (also known as the Polder tensor) in the case of  $H_z = 0$  have been studied previously.<sup>25,27,32</sup> In these works, the nanotube is in a circular magnetic configuration  $\Theta_0 = \pi/2$ , for which the asymmetries in dispersion relation are the consequence of the curvature-induced broken mirror symmetry of the dynamic volume charges. The SW wave numbers are given by the mode  $n$  and wave vector  $k_z$ , both of them describing the SW phase distribution along the azimuthal  $\hat{\varphi}$  direction and along the  $\hat{z}$  direction, respectively. It has been shown that the dispersion relation is degenerated in the sign of  $n$ , hence the SWs form azimuthal standing waves with  $2|n|$  nodal lines. With the application of a longitudinal magnetic field  $H_z \neq 0$ , the frequency degeneration regarding the sign of  $n$  is broken, consequently the formation of azimuthal standing waves is disrupted and conditions to observe separately individual azimuthal modes on the nanotube mantle is therefore possible, as we see later.

Detailed derivations of  $f[n, k_z]$  and  $\aleph_{k_z}^n$  with the inclusion of  $H_z \neq 0$ , as well as, analytical calculations on the impedance response of the CPW system ( $Z_1^{(\text{Tot})}[\omega]$  and  $Z_2^{(\text{Tot})}[\omega]$ ), are presented in the supplementary material.<sup>33</sup> Nevertheless, for a better understanding of the manuscript the main results are written next. Accordingly, the dispersion relation is given as  $\omega_{k_z}^n = \omega_{M_s}(\mathcal{A}_{k_z}^n + \sqrt{\mathcal{B}_{k_z}^n \mathcal{C}_{k_z}^n})$  and the dynamic susceptibility as

$$\aleph_{k_z}^n = \begin{pmatrix} \chi_{\rho\rho}^{n, k_z} & \chi_{\rho v}^{n, k_z} \\ -\chi_{\rho v}^{n, k_z} & \chi_{vv}^{n, k_z} \end{pmatrix} = \begin{pmatrix} \frac{i\mathbb{B}}{\mathbb{A}^2 + \mathbb{B}\mathbb{C}} & \frac{i\mathbb{A}}{\mathbb{A}^2 + \mathbb{B}\mathbb{C}} \\ -\frac{i\mathbb{A}}{\mathbb{A}^2 + \mathbb{B}\mathbb{C}} & \frac{i\mathbb{C}}{\mathbb{A}^2 + \mathbb{B}\mathbb{C}} \end{pmatrix}, \quad (1)$$

where  $\omega_{M_s} = \gamma M_s$ ,  $\mathbb{A} \equiv \omega - \gamma M_s \mathcal{A}_{k_z}^n$ ,  $\mathbb{B} \equiv -\alpha_G \omega + i\gamma M_s \mathcal{B}_{k_z}^n$ ,  $\mathbb{C} \equiv -\alpha_G \omega + i\gamma M_s \mathcal{C}_{k_z}^n$  and  $\gamma = \mu_0 \gamma_0$ , with  $\mathcal{A}_{k_z}^n$ ,  $\mathcal{B}_{k_z}^n$ , and  $\mathcal{C}_{k_z}^n$  given as

$$\begin{aligned} \mathcal{A}_{k_z}^n &= \mathcal{K}_{k_z}^n \sin \Theta_0 - \mathcal{N}_{k_z}^n \cos \Theta_0, \\ \mathcal{B}_{k_z}^n &= h_0 \sin \Theta_0 + h_z \cos \Theta_0 + h_u \cos[2\Theta_0] + (n^2 h_u + l_{ex}^2 k_z^2) \\ &\quad + (\mathcal{L}_{k_z}^n \sin^2 \Theta_0 - \mathcal{M}_{k_z}^n \sin[2\Theta_0] + \mathcal{O}_{k_z}^n \cos^2 \Theta_0), \\ \mathcal{C}_{k_z}^n &= h_0 \sin \Theta_0 + h_z \cos \Theta_0 + h_u \cos^2 \Theta_0 + (n^2 h_u + l_{ex}^2 k_z^2) \\ &\quad + \mathcal{J}_{k_z}^n, \end{aligned} \quad (2)$$

where  $h_z \equiv H_z/M_s$ ,  $h_0 \equiv H_0/M_s$ ,  $h_u \equiv H_u/M_s$ ,  $\gamma_0 = g\mu_B/\hbar$  is the gyromagnetic ratio,  $g$  is the electron's Landé-factor,  $\mu_B$  is the Bohr magneton,  $\hbar$  is the Planck constant,  $l_{\text{ex}} = \sqrt{A/K_d}$  is the exchange length,  $A$  is the stiffness constant,  $\mu_0$  is the vacuum magnetic permeability and  $\alpha_G$  is the Gilbert damping. The terms denoted by  $\mathcal{J}$ ,  $\mathcal{K}$ ,  $\mathcal{L}$ ,  $\mathcal{M}$ ,  $\mathcal{N}$ ,  $\mathcal{O}$  are hyper geometrical functions that depend on the nanotube radius  $R$  and thickness  $d$  (the inner radius defined as  $r = R - d$ ) and represent the normalized dynamic dipolar field contributions.

The inclusion of  $H_z \neq 0$  is reflected in the dependence on  $\Theta_0$  of the normalized stiffness fields  $\mathcal{A}_{k_z}^n$ ,  $\mathcal{B}_{k_z}^n$  and  $\mathcal{C}_{k_z}^n$ , and in the term  $h_z \cos \Theta_0$  in  $\mathcal{B}_{k_z}^n$  and  $\mathcal{C}_{k_z}^n$ . Note that  $\mathcal{A}_{k_z}^n$  is the magnetochiral stiffness field arising from the nanotube curvature, whereas  $\mathcal{B}_{k_z}^n$  and  $\mathcal{C}_{k_z}^n$  constitute the stiffness fields along the  $\hat{\rho}$  and  $\hat{\varphi}$  directions, respectively.<sup>32</sup>

$Z_1^{(\text{Tot})}[\omega]$  ( $Z_2^{(\text{Tot})}[\omega]$ ) denote the induced impedance in CPW1 (CPW2) due to the electromagnetic coupling between the CPW1 (CPW2) and SWs when are excited in the nanotube with the CPW2 (CPW1). These impedances are given as

$$Z_x^{(\text{Tot})}[\omega] = (2\pi)^3 S \mu_0 \omega \sum_{n=-\infty}^{\infty} \int_0^{\infty} dk_z z_x^{(n)}[k_z, \omega] \quad (3)$$

where  $z_1^{(n)}[k_z, \omega]$  ( $z_2^{(n)}[k_z, \omega]$ ) (see equations 22 at Suppl. Mat.<sup>33</sup> for the full expression) denotes the induced impedance on CPW1 (CPW2) due to the coupling to a single SW mode  $n$  with wave vector  $k_z$  at an angular frequency  $\omega$  that is excited in CPW2 (CPW1).  $z_1^{(n)}[k_z, \omega]$  and  $z_2^{(n)}[k_z, \omega]$  depends explicitly on the dynamic susceptibility components  $\chi_{xy}^{n, k_z}$  (with  $x$  and  $y$  running on  $\rho$ ,  $\varphi$  and  $z$ ), and on the Fourier decomposition  $h_{x, \text{rf}}^n[k_z]$  (with  $x = \rho, \varphi, z$ ) of the rf-magnetic field components  $\vec{h}_{x, \text{rf}}$  created by each one of the CPWs. This decomposition is performed in the Fourier space defined by the wavevector numbers  $\{n, k_z\}$ , therefore giving information of the modes  $n$  and wave vectors  $k_z$  that are most likely to be excited on the nanotube. Under the approach of a thin MNT (in such a way that SWs have a homogeneous radial phase along the nanotube thickness), the rf-magnetic field in the Fourier space is written as  $\vec{H}^{(n)}[k_z] = \sum_{x=\rho, \varphi, z} \hat{x} H_x^{(n)}[k_z]$ , where  $H_x^{(n)}[k_z] \equiv \langle h_{\text{rf}} \rangle_x^n[k_z]/I_{\text{rf}}$  with  $x = \rho, \varphi, z$ , where  $\langle h_{\text{rf}} \rangle_x^n[k_z] = (2\pi/S) \int_r^R h_{x, \text{rf}}^n[k_z] \rho d\rho$  is the rf-field averaged in the nanotube thickness, whereas  $I_{\text{rf}}$  is the current of amplitude of the rf-electrical current injected to the CPWs at an oscillation frequency  $\omega/(2\pi)$ .

The rf-field distribution produced by the CPW in the Fourier space  $\{n, k_z\}$  is shown in Figure 2. A main maximum peak is observed at  $k_z = k_1 = 5.5 \text{ rads}/\mu\text{m}$  and  $n = \pm 1$ , and with a width of  $\Delta k_z = 7.5 \text{ rads}/\mu\text{m}$ . This peak is in agreement with the literature (a maximum peak around  $k_z \approx \pi/(2w)$  is expected).<sup>38-40</sup>

Using our model of the impedance induced by the SWs at the CPWs (see equation 3), we can predict the SW

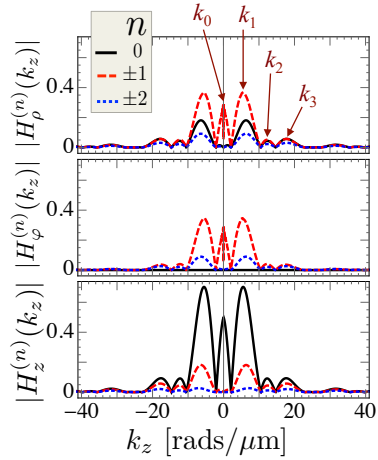


FIG. 2. (Color online). Wave vector distributions created by of one CPW on the NT mantle. A radio-frequency current  $I_{\text{RF}}$  is injected to one CPW, inducing the magnetic fields  $H_\rho[\vec{r}]$ ,  $H_\varphi[\vec{r}]$  and  $H_z[\vec{r}]$  at the nanotube mantle. Here  $(\rho, \varphi, z)$  are the cylindrical coordinates. A Fourier transformation of  $H_\rho[\vec{r}]$ ,  $H_\varphi[\vec{r}]$  and  $H_z[\vec{r}]$  produces the fields in the Fourier space  $H_\rho^{(n)}[k_z]$ ,  $H_\varphi^{(n)}[k_z]$ , and  $H_z^{(n)}[k_z]$ . These fields show the wave vector distribution denoted by the azimuthal SW mode  $n$  and SW wave vector along the nanotube large axis  $k_z$ . Representative peaks of the vector distribution are mostly given at  $n = 0, \pm 1, \pm 2$  and  $k_z$  with values of  $|k_z| \in \{k_0, k_1, k_2, k_3\} = \{0, 5.5, 12.1, 17.5\} \text{ rads}/\mu\text{m}$ . The geometrical dimensions of the CPWs are  $w = \text{GAP} = 250 \text{ nm}$  and a separation of  $s = 5 \mu\text{m}$  between the two CPW centers. The nanotube dimensions are 210 nm in diameter, 10 nm in thickness and 15  $\mu\text{m}$  in length.

impedance spectrum as a function of the applied magnetic field  $H_z$ , as shown in figure 3. Here, the color-code represents the imaginary part  $Z_{1, \text{Im}}^{(\text{Tot})}$  and  $Z_{2, \text{Im}}^{(\text{Tot})}$  of the predicted impedances  $Z_1^{(\text{Tot})}$  and  $Z_2^{(\text{Tot})}$ , respectively. In these predictions, we can track the impedance resonances to reciprocal and nonreciprocal SWs by super imposing the SW eigenfrequencies  $f[n, k_z]$ . The strongest impedance signals are consistent with the larger peaks from the rf-field distribution (see figure 2). Such peaks correspond to the modes  $n = 0, \pm 1$  and are centered at the wave vectors  $k_z = k_0, \pm k_1$ , with  $k_0 = 0$  and  $k_1 = 5.5 \text{ rads}/\mu\text{m}$ . Note that the Kittel FMR mode, corresponding to the SW with  $k_z = 0$  and  $n = 0$  (black-dotted curve), can be resolved and is reciprocal as expected, i.e.,  $Z_{1, \text{Im}}^{(\text{Tot})}$  and  $Z_{2, \text{Im}}^{(\text{Tot})}$  do not show a frequency shift at  $\{n, k_z\} = \{0, 0\}$ , as expected. Total reciprocity in the next order mode  $n = \pm 1$  at  $k_z = 0$  is also predicted by impedance calculations (red curve). Notorious nonreciprocities are presented for SWs with non-zero wave vector,  $k_z \neq 0$ , which is consistent with the nonreciprocal term  $\mathcal{A}_{k_z}^n$  (at  $k_z \neq 0$  the term  $\mathcal{A}_{k_z}^n \neq 0$ , thus the curvature-induced nonreciprocity is non-zero). Under this condition, nonreciprocities can be observed by comparing the case  $\{n, k_z\}$  to  $\{-n, -k_z\}$  between the

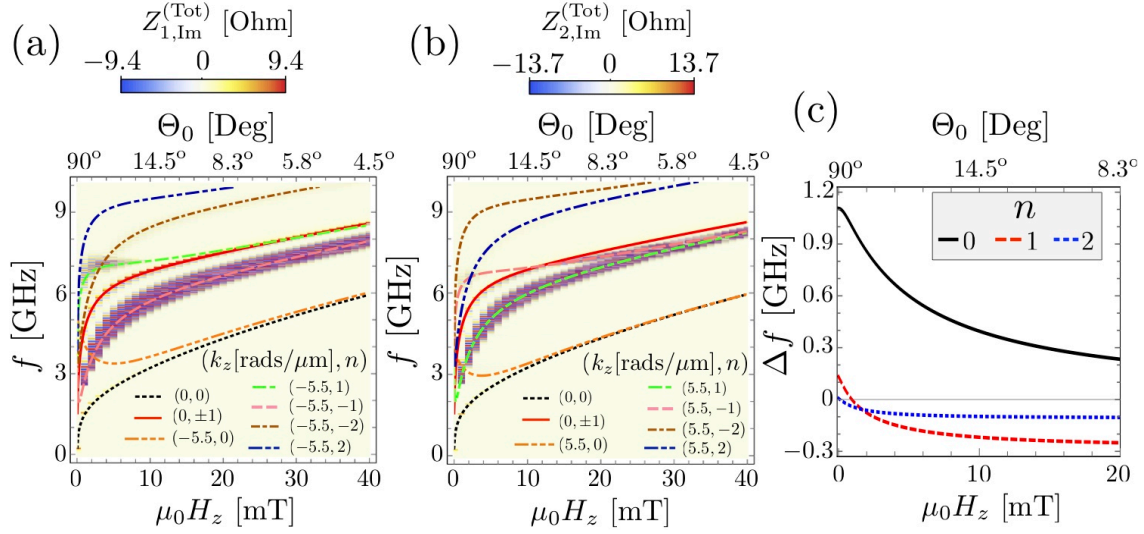


FIG. 3. (Color online). (a),(b) Impedance  $Z_{1,\text{Im}}^{(\text{Tot})}$  ( $Z_{2,\text{Im}}^{(\text{Tot})}$ ) induced in CPW1 (CPW2) by exciting SWs in the MNT with CPW2 (CPW1) in function of RF frequency and applied magnetic field  $H_z$ . Asymmetric frequency can be noticed in cases of  $k_z \neq 0$ . The curvature-induced asymmetries in the frequency linewidth are also responsible for the differences between maximum values of the induced impedances  $Z_{1,\text{Im}}^{(\text{Tot})}$  and  $Z_{2,\text{Im}}^{(\text{Tot})}$ . c) Frequency asymmetry  $\Delta f$  as function of the applied field  $H_z$  for  $k_z = k_1 = 5.5$  rads/ $\mu\text{m}$  and modes  $n = 0, 1, 2$ . A permalloy nanotube of 210 nm diameter, 10 nm thickness and 0.001 Gilbert damping are assumed. Calculations are shown for a long enough MNT in order to neglect the contributions of the MNT ends to the predicted impedances.

SW spectrums  $Z_{1,\text{Im}}^{(\text{Tot})}$  and  $Z_{2,\text{Im}}^{(\text{Tot})}$ . Specifically, nonreciprocities can be observed for  $|k_z| = k_1 = 5.5$  rads/ $\mu\text{m}$  and  $|n| = 0, 1, 2$ , and the quantification of the frequency asymmetries  $\Delta f \equiv f[n, k_z] - f[-n, -k_z]$  (for those wavevectors that are resolved by the SW impedance spectrum figure 2)) as function of  $H_z$  are presented in figure 3c). A maximum frequency shift of approximately 1.1 GHz can be resolved for  $|n| = 0$  at  $H_z = 0$ , as expected. Note that impedance values for  $n = 0, \pm 2$  and  $|k_z| = k_1$  are at the order of  $10^{-2}$  Ohms, therefore can only be slightly resolved by the color-code scale of  $Z_{1,\text{Im}}^{(\text{Tot})}$  and  $Z_{2,\text{Im}}^{(\text{Tot})}$  at figure 3a,b). In general, we estimate that, for  $|n| \in (0, 1, 2)$ ,  $\Delta f$  goes from (1.1, 0.15, 0) GHz at  $\mu_0 H_z = 0$  to (0.2, -0.25, -0.1) GHz at  $\mu_0 H_z = 20$  mT. Note the change of sign of  $\Delta f$  that occur at  $\mu_0 H_z \approx 1$  mT for  $|k_z| = k_1 = 5.5$  rads/ $\mu\text{m}$  and  $|n| = 1$  (see the red dashed curve in figure 3c). For this wavenumbers, the asymmetry shows a total variation of 0.4 GHz. This value can be increased up to the GHz range by accessing larger wave vectors. For instance, a total variation of approximately 0.8 GHz (1.2 GHz) in the frequency asymmetry is predicted for  $|n| = 1$  and  $|k_z| = 12$  rads/ $\mu\text{m}$  ( $|k_z| = 18$  rads/ $\mu\text{m}$ ). These wave vectors can be, in principle, excited with the proposed CPWs size, as shown in figure 2. In this figure, a small peak with  $|n| = 1$  and  $k_z = k_2 = 12.1$  rads/ $\mu\text{m}$  ( $k_z = k_3 = 17.5$  rads/ $\mu\text{m}$ ) can be excited in the nanotube, as indeed occurs; however, the predicted amplitude of the impedance at these wavenumbers is of the order of  $10^{-3}$  Ohms, which might

be challenging to be resolved with a Vector Network Analyzer setup.

It is important to comment on the total SWs wavelength ( $\lambda = 2\pi/k$ ) that could be excited/measured on the MNT using the CPWs. Indeed, our predictions show that the curved topology of MNTs would allow exciting SWs with large (micrometer) and short (sub-micrometer) wavelengths  $\lambda = 2\pi/k$ , where  $k = \sqrt{k_z^2 + \bar{k}_\varphi^2}$  is the total wave vector magnitude and  $\bar{k}_\varphi = n/\bar{\rho}$  is the azimuthal wave vector. Hence, for those wavenumbers that can be resolved by the impedance spectrum, a micrometer wavelength  $\lambda = 1.14$   $\mu\text{m}$  is obtained for  $|k_z| = k_1$  and  $n = 0$ , whereas the shortest wavelength  $\lambda = 300$  nm is given for  $|k_z| = k_1$  and  $|n| = 2$ . Notice that the wavelength can be reduced even further to  $\lambda = 240$  nm in the case that the mode  $|n| = 2$  and wave vector  $|k_z| = k_3$  can be resolved.

We have calculated the optimized parameters of a magnonic device that can be further implemented to confirm for the first time the curvature-induced nonreciprocal SW dispersion relation. Asymmetries in the SW dispersion at the GHz range, at sub-micrometer wavelengths and on-demand controllability on its curvature-induced nonreciprocal properties have been predicted for the given parameters. Moreover, we have shown that the application of an external field  $H_z$  breaks the SW frequency degeneration regarding the sign of the mode number  $n$ , therefore allowing the excitation of SWs with wavelength down to  $\lambda = 240$  nm, as well as, the observation of individual modes with the CPW setup.

In the context of magnonic applications, our results

might encourage further developments in the emerging field of 3D magnon devices using curved magnetic membranes, for instance, for improving the capabilities of transferring information at few hundred nanometers SW wavelength encoded simultaneously in the mode number  $n$  and wave vector  $k_z$ , and in the development of unidirectional SWs waveguides and magnetochiral magnonic crystals.

## AUTHOR CONTRIBUTIONS

J.A.O developed the analytical model and wrote the manuscript. All authors interpreted and discussed the results and co-wrote the manuscript.

## ADDITIONAL INFORMATION

The authors declare no competing financial interests. Reprints and permission information is available online at <http://xxxxxxxxxx>. Correspondence and requests for materials should be addressed to J.A.O.

## REFERENCES

- <sup>1</sup>B. Hoefflinger, in *Chips 2020* (Springer, 2011) pp. 161–174.
- <sup>2</sup>A. V. Chumak, V. I. Vasyuchka, A. A. Serga, and B. Hillebrands, *Nat Phys* **11**, 453 (2015).
- <sup>3</sup>S. A. Nikitov, D. V. Kalyabin, I. V. Lisenkov, A. Slavin, Y. N. Barabanenkov, S. A. Osokin, A. V. Sadovnikov, E. N. Beginin, M. A. Morozova, Y. A. Filimonov, Y. V. Khivintsev, S. L. Vysotsky, V. K. Sakharov, and E. S. Pavlov, *Physics-Uspekhi* **58**, 1002 (2015).
- <sup>4</sup>M. M. Waldrop, *Nature News* **530**, 144 (2016).
- <sup>5</sup>A. V. Chumak, A. A. Serga, and B. Hillebrands, *Journal of Physics D: Applied Physics* **50**, 244001 (2017).
- <sup>6</sup>Y. Tserkovnyak, A. Brataas, and G. E. Bauer, *Physical review letters* **88**, 117601 (2002).
- <sup>7</sup>Y. Kajiwara, K. Harii, S. Takahashi, J.-i. Ohe, K. Uchida, M. Mizuguchi, H. Umezawa, H. Kawai, K. Ando, K. Takanashi, *et al.*, *Nature* **464**, 262 (2010).
- <sup>8</sup>M. Madami, S. Bonetti, G. Consolo, S. Tacchi, G. Carlotti, G. Gubbiotti, F. Mancoff, M. A. Yar, and J. Åkerman, *Nature nanotechnology* **6**, 635 (2011).
- <sup>9</sup>C. W. Sandweg, Y. Kajiwara, A. V. Chumak, A. A. Serga, V. I. Vasyuchka, M. B. Jungfleisch, E. Saitoh, and B. Hillebrands, *Phys. Rev. Lett.* **106**, 216601 (2011).
- <sup>10</sup>V. E. Demidov, S. Urazhdin, H. Ulrichs, V. Tiberkevich, A. Slavin, D. Baither, G. Schmitz, and S. O. Demokritov, *Nature materials* **11**, 1028 (2012).
- <sup>11</sup>A. V. Chumak, A. A. Serga, and B. Hillebrands, *Nature communications* **5** (2014).
- <sup>12</sup>K. Vogt, F. Fradin, J. Pearson, T. Sebastian, S. Bader, B. Hillebrands, A. Hoffmann, and H. Schultheiss, *Nature communications* **5** (2014).
- <sup>13</sup>A. V. Sadovnikov, C. S. Davies, S. V. Grishin, V. Kruglyak, D. Romanenko, Y. P. Sharaevskii, and S. Nikitov, *Applied Physics Letters* **106**, 192406 (2015).
- <sup>14</sup>J. Lan, W. Yu, R. Wu, J. Xiao, *et al.*, *Physical Review X* **5**, 041049 (2015).
- <sup>15</sup>S. Klingler, P. Pirro, T. Brächer, B. Leven, B. Hillebrands, and A. V. Chumak, *Applied Physics Letters* **105**, 152410 (2014).
- <sup>16</sup>I. Radu, O. Zografos, A. Vaysset, F. Ciubotaru, J. Yan, J. Swerts, D. Radisic, B. Briggs, B. Soree, M. Manfrini, *et al.*, in *Electron Devices Meeting (IEDM), 2015 IEEE International* (IEEE, 2015) pp. 32–5.
- <sup>17</sup>A. Khitun and K. L. Wang, *Journal of Applied Physics* **110**, 034306 (2011).
- <sup>18</sup>T. Brächer, F. Heussner, P. Pirro, T. Meyer, T. Fischer, M. Geilen, B. Heinz, B. Lägel, A. Serga, and B. Hillebrands, *Scientific reports* **6**, 38235 (2016).
- <sup>19</sup>C. J. Tock and J. F. Gregg, *arXiv preprint arXiv:1804.05575* (2018).
- <sup>20</sup>G. Talmelli, F. Ciubotaru, K. Garello, X. Sun, M. Heyns, I. P. Radu, C. Adelmann, and T. Devolder, *arXiv preprint arXiv:1802.00861* (2018).
- <sup>21</sup>J. Otálora, D. Cortés-Ortuño, D. Görlitz, K. Nielsch, and P. Landeros, *Journal of Applied Physics* **117**, 173914 (2015).
- <sup>22</sup>H. Salinas, J. Restrepo, and Ó. Iglesias, *Scientific reports* **8** (2018).
- <sup>23</sup>R. Hertel, in *Spin*, Vol. 3 (World Scientific, 2013) p. 1340009.
- <sup>24</sup>Y. Gaididei, V. P. Kravchuk, and D. D. Sheka, *Phys. Rev. Lett.* **112**, 257203 (2014).
- <sup>25</sup>J. A. Otálora, M. Yan, H. Schultheiss, R. Hertel, and A. Kákay, *Physical review letters* **117**, 227203 (2016).
- <sup>26</sup>R. Streubel, P. Fischer, F. Kronast, V. P. Kravchuk, D. D. Sheka, Y. Gaididei, O. G. Schmidt, and D. Makarov, *Journal of Physics D: Applied Physics* **49**, 363001 (2016).
- <sup>27</sup>J. A. Otálora, M. Yan, H. Schultheiss, R. Hertel, and A. Kákay, *Phys. Rev. B* **95**, 184415 (2017).
- <sup>28</sup>A. Fernández-Pacheco, R. Streubel, O. Fruchart, R. Hertel, P. Fischer, and R. P. Cowburn, *Nature Communications* **8**, 15756 (2017).
- <sup>29</sup>M. Stano and O. Fruchart, *Handbook of Magnetic Materials* **27**, 155 (2018).
- <sup>30</sup>D. D. Sheka, V. P. Kravchuk, K. V. Yershov, and Y. Gaididei, *Phys. Rev. B* **92**, 054417 (2015).
- <sup>31</sup>Y. Gaididei, A. Goussev, V. P. Kravchuk, O. V. Pylypovskiy, J. M. Robbins, D. D. Sheka, V. Slastikov, and S. Vasylkeyvych, *Journal of Physics A: Mathematical and Theoretical* **50**, 385401 (2017).
- <sup>32</sup>J. A. Otálora, A. Kákay, J. Lindner, H. Schultheiss, A. Thomas, J. Fassbender, and K. Nielsch, *Phys. Rev. B* **98**, 014403 (2018).
- <sup>33</sup>“See supplemental material at [url will be inserted by publisher] for equations derivation.”.
- <sup>34</sup>P. Landeros, O. J. Suárez, A. Cuchillo, and P. Vargas, *Phys. Rev. B* **79**, 024404 (2009).
- <sup>35</sup>M. Wyss, A. Mehlin, B. Gross, A. Buchter, A. Farhan, M. Buzzi, A. Kleibert, G. Tütüncüoglu, F. Heimbach, A. Fontcuberta i Morral, D. Grundler, and M. Poggio, *Phys. Rev. B* **96**, 024423 (2017).
- <sup>36</sup>M. Staño, S. Schaefer, A. Wartelle, M. Rioult, R. Belkhou, A. Sala, T. O. Menteş, A. Locatelli, L. Cagnon, B. Trapp, *et al.*, *SciPost Physics* **5**, 038 (2018).
- <sup>37</sup>M. Zimmermann, T. N. G. Meier, F. Dirnberger, A. Kákay, M. Decker, S. Wintz, S. Finizio, E. Josten, J. Raabe, M. Kronseder, *et al.*, *Nano letters* **18**, 2828 (2018).
- <sup>38</sup>G. F. Dürr, *Spin Waves in Nanochannels, Created by Individual and Periodic Bi-Component Ferromagnetic Devices*, Ph.D. thesis, Technische Universität München (2012).
- <sup>39</sup>T. Schwarze, *Spin waves in 2D and 3D magnonic crystals: from nanostructured ferromagnetic materials to chiral helimagnets*, Ph.D. thesis, Technische Universität München (2013).
- <sup>40</sup>V. Vlaminck and M. Bailleul, *Physical Review B* **81**, 014425 (2010).